Full Text View

Volume 29, Issue 9 (September 1999)

Journal of Physical Oceanography
Article: pp. 2419–2431 | Abstract | PDF (402K)

Effects of Stratification and Bottom Topography on the Kuroshio Path Variation South of Japan. Part I: Dependence of the Path Selection on Velocity

Shuhei Masuda, Kazunori Akitomo, and Toshiyuki Awaji

Department of Geophysics, Graduate School of Science, Kyoto University, Kyoto, Japan

(Manuscript received April 28, 1998, in final form September 10, 1998)

DOI: 10.1175/1520-0485(1999)029<2419:EOSABT>2.0.CO;2

ABSTRACT

Numerical experiments are executed using a two-layer inflow–outflow ocean model with simplified geometry to investigate the effects of stratification and bottom topography on the path variation of the Kuroshio south of Japan. In a flat-bottom ocean, the dependence of the Kuroshio path selection on its inflow velocity V_{max} is basically the same as in a barotropic ocean, that is, the Kuroshio takes a straight path at low V_{max} (regime I), a meandering path at high V_{max} (regime II), and both paths at intermediate V_{max} (regime III: multiple equilibrium state). However, the range of regime III shifts to higher V_{max} by 0.10~0.30 m s^{-1}. Stratification causes and maintains the offshore shift of the current path south of Kyushu through the conservation of potential vorticity. As a result, a small meander stagnates southeast of Kyushu, not developing into a large meander even for higher V_{max} since the vorticity supply from the coast is reduced. For the same reason, higher V_{max} is needed to maintain a meandering path. Bottom topographic features such as a continental slope and ridge significantly change the path selection. A straight path appears for the whole experimental range of V_{max} and a meandering path only exists at intermediate V_{max}. The continental slope along the southern coast of Japan captures the main flow to permit a straight path for all V_{max}. Further, the Izu Ridge inhibits a meandering path hanging over the western flank of the ridge and narrows the range of V_{max} in which the meandering state exists. The transition induced by monotonic changes of V_{max} is significantly affected for a jump from a straight to a meandering path but not affected as much for a reverse jump. In a flat-bottom ocean, the enlargement of a small meander due to baroclinicity causes a quick transition from a straight to a meandering path with a large velocity change while the transition is impeded for a small velocity change. No transition occurs by a monotonic increase in V_{max} with bottom topography since a straight path can exist for all V_{max}.

1. Introduction

The Kuroshio, the western boundary current in the North Pacific, has three relatively stable paths south of Japan (e.g., Kawabe 1985): a nearshore non-large-meander path (hereafter called a straight path) flowing along the southern coast of Japan, an offshore non-large-meander path (a C-type path) passing south of Hachijo Island, and a large meander path (a meandering path) largely detouring southward off Enshunada. The variations among these paths on timescales of years to decades (e.g., Kawabe 1985, 1987; Kutsuwada 1988) are also remarkable. During the transition from a straight to a meandering path, a small meander formed southeast of Kyushu progresses eastward along the southern coast of Japan to develop into a large meander off Enshunada (e.g., Shoji 1972). It takes 3 or 4 months. To the contrary, the transition from a meandering to a straight path takes over a half year via a C-type path (Shoji 1964; Nitani 1977; Nishida 1982).

The volume transport or velocity has been considered to be one of the crucial factors for these path variations. Some observational studies showed that the volume transport south of Japan is small when the Kuroshio takes a meandering path (e.g., Nitani 1972, 1975). Others reported that it is large in the upstream regions (the East China Sea or the Tokara Strait south of Kyushu) when a meandering path occurs (e.g., Nitani 1972; Kawabe 1980; Saiki 1982; Nishizawa et al. 1982). These conflicting results may be because of uncertainties of the reference level for dynamic calculation and estimation of the recirculating transport (Saiki 1985). Qiu and Joyce (1992) pointed out that the eastward volume transport based on dynamic calculation south of Japan exhibits no significant changes between straight-path and meander-path years, but that the net transport of the Kuroshio excluding the contribution of recirculations shows a 30% increase during the meander-path years. A decisive conclusion has not been obtained so far about the dependence of the path selection on the volume transport.

Many theoretical and experimental studies also have made efforts to reveal the relationship between the Kuroshio path variation and its transport. White and McCreary (1976) were the first to point out the possibility that a meandering path is a Rossby lee wave formed behind Kyushu. According to them, the Kuroshio takes a meandering (straight) path when its transport is small (large) and the wavelength becomes shorter (larger) than the distance between Kyushu and the Izu Ridge. Masuda (1982) found that a multiple equilibrium regime with both straight and meandering paths can exist. This has been confirmed by numerical experiments with an inflow–outflow ocean model (Chao 1984;Yasuda et al. 1985; Yoon and Yasuda 1987; Akitomo et al. 1991) and its reality has been recently suggested by observational studies (Obata 1993; Kawabe 1995). In numerical experiments with a realistic inclination of the south coast of Japan, a straight path appears at low velocities, a meandering path at high velocities, and a multiple equilibrium regime at intermediate velocities. The transition from a straight (meandering) path to a meandering (straight) path occurs when the velocity exceeds (falls below) a critical value over (below) which a straight (meandering) path cannot exist. Particularly, Akitomo et al. (1991) has revealed that the geometry of Kyushu is essential to the transition process from a straight to a meandering path during which a small meander formed by the separation of flow southeast of Kyushu progresses eastward along the south coast of Japan to develop into a large meander.

However, recent observational studies suggested another possibility that a short-term increase in velocity may be related to transitions between a straight and a meandering path (Mizuno et al. 1990; Obata 1993; Kawabe 1995; Akitomo et al. 1996). Further, Kawabe (1995) found that both straight and meandering paths appear with an equal probability at intermediate and high velocities in the Tokara Strait while only a straight path appears at low velocities. This means that the path transition from a straight to a meandering path never occurs in a manner that previous model studies predicted.

Investigating this problem with a barotropic ocean model, Akitomo et al. (1997) showed that a short-term increase in the Kuroshio velocity (pulselike variation superimposed on an otherwise constant velocity) can cause the formation of a progressive small meander southeast of Kyushu and lead to the transition from a straight to a meandering path in the multiple equilibrium regime. However, the reverse transition was not reproduced with a similar velocity increase. They speculated that other physical factors such as stratification and bottom topography may be essential to the transition process from a meandering to a straight path. Indeed, it has been reported that the continental slope south of Japan and bottom topography around the Izu Ridge are closely related to the path variation (e.g., Robinson and Taft 1972; Sekine 1990) and that the structure of the Kuroshio flow is strongly controlled by bottom topography, such as the Izu Ridge (e.g., Endoh 1978; Nishida 1982;Kawabe 1985). Sekine and Toba (1981) indicated that bottom topography also plays a significant role in the formation of the small meander southeast of Kyushu.

Hence, the purpose of our study is to clarify the effects of stratification and bottom topography on the Kuroshio path variation, including path transitions due to a short-term velocity change, by using a two-layer inflow–outflow model. In Part I, we will first investigate their effects on the Kuroshio path selection and the path transitions caused by a monotonic velocity change (a linear change from one $V_{\max}$ to another $V_{\max}$). In Part II (Masuda and Akitomo 1999), our attention will be focused on these effects on the path transitions triggered by a short-term velocity change.

2. Numerical experiment

A two-layer inflow–outflow ocean model with coastal geometry and bottom topography is used (Fig. 1). The coastal geometry is the same as in Akitomo et al. (1997, hereafter AMA97) and the simplified bottom topography south of Japan is added, including the continental slope from the East China Sea to south of Japan and the Izu Ridge of 240-km width perpendicular to the south coast of Japan. Further, the model ocean has a 500-km-wide buffering region to the east to prevent computational errors, which are generated around the outlet, from penetrating into the domain of interest. For this purpose, the horizontal eddy viscosity is linearly increased tenfold of the interior value at its eastern end (5×10^7 m^2 s^{-1}). The governing equations are two-layer primitive equations on a β plane under the assumption of the hydrostatic balance, the Boussinesq and rigid-lid approximation. The momentum equations in the upper and lower layers are given as

$$\frac{\partial u_1}{\partial t} + u_1\frac{\partial u_1}{\partial x} + v_1\frac{\partial u_1}{\partial y} - fv_1 = -\frac{1}{\rho_0}\frac{\partial p_s}{\partial x} + \nu_H\nabla_H^2 u_1, \quad (1)$$

$$\frac{\partial v_1}{\partial t} + u_1\frac{\partial v_1}{\partial x} + v_1\frac{\partial v_1}{\partial y} + fu_1 = -\frac{1}{\rho_0}\frac{\partial p_s}{\partial y} + \nu_H\nabla_H^2 v_1 \quad (2)$$

and

$$\frac{\partial u_2}{\partial t} + u_2\frac{\partial u_2}{\partial x} + v_2\frac{\partial u_2}{\partial y} - fv_2 = -\frac{1}{\rho_0}\frac{\partial p_s}{\partial x} + \frac{\Delta\rho}{\rho_0}g\frac{\partial \eta}{\partial x} + \nu_H\nabla_H^2 u_2, \quad (3)$$

$$\frac{\partial v_2}{\partial t} + u_2\frac{\partial v_2}{\partial x} + v_2\frac{\partial v_2}{\partial y} + fu_2 = -\frac{1}{\rho_0}\frac{\partial p_s}{\partial y} + \frac{\Delta\rho}{\rho_0}g\frac{\partial \eta}{\partial y} + \nu_H\nabla_H^2 v_2. \quad (4)$$

The continuity equations in the upper and lower layers are written as

$$\frac{\partial \eta}{\partial t} + \frac{\partial (h_1 + \eta)u_1}{\partial x} + \frac{\partial (h_1 + \eta)v_1}{\partial y} = 0 \quad (5)$$

and

$$\frac{\partial \eta}{\partial t} - \frac{\partial (D - h_1 - \eta)u_2}{\partial x} - \frac{\partial (D - h_1 - \eta)v_2}{\partial y} = 0. \quad (6)$$

In these equations, (u, v) are the horizontal velocity components in the (x, y) directions, g is the acceleration due to gravity, p_s the sea surface pressure, ρ_0 the mean water density, $\Delta\rho$ the density difference between the two layers, η the interfacial displacement (downward positive), D the total depth, h_1 the upper-layer thickness at rest, and ν_H the horizontal eddy viscosity. The subscripts 1 and 2 denote quantities in the upper and lower layers, respectively. The horizontal Laplacian operator ∇^2_H is defined by $\partial^2/\partial x^2 + \partial^2/\partial y^2$. The Coriolis parameter f is given by

$$f = f_0 + \beta(x\sin\theta + y\cos\theta), \quad (7)$$

where f_0 is the reference value, β the beta parameter (the meridional gradient of f), and θ the inclination angle of the southern coast of Japan from the zonal direction.

The Kuroshio is driven by inflow at the southwest corner and outflow at the northeast corner, and is assumed to be a geostrophic current confined within the upper layer. Then, the velocity components at the outlet are given by

$$(u_1, v_1) = \left(-\frac{g'}{f}\frac{\partial \eta}{\partial y}, 0\right)$$
$$(u_2, v_2) = (0, 0), \qquad (8)$$

where $g' = \Delta\rho g/\rho_0$ is the reduced gravity. The boundary value of η is determined from Eq. (8), assuming that the outflow velocity has a triangular profile with a maximum value of V_{max} (Fig. 1) and that η is zero at the southern end of the outlet. Similar conditions are imposed at the inlet,

$$\left(\frac{\partial u_1}{\partial y}, v_1\right) = \left(0, \frac{g'}{f}\frac{\partial \eta}{\partial x}\right)$$
$$(u_2, v_2) = (0, 0). \qquad (9)$$

Here η is determined so that the inlet volume transport and velocity profile are the same as at the outlet. Accordingly, the value of η at the inlet is different from that at the outlet because f is different. Though the value of u_1 is not specified at the inlet for stable numerical calculation, it is almost zero. Surface, bottom, and interfacial stresses are not included at all, while a no-slip condition is imposed at all lateral boundaries. The maximum total depth D_0 and the upper-layer thickness at rest h_1 are 4000 m and 800 m, respectively, and $\Delta\rho$ is 3.0 kg m^{-3}. Other physical parameters are the same as in AMA97 (Table 1).

The initial condition and the method of numerical integration are also the same as in AMA97. Experiments are first executed with a flat-bottom model ocean in order to investigate the effect of stratification (hereafter FB case). After that, we turn to a model ocean including bottom-topographic features such as the continental slope south of Japan and the Izu Ridge (BT case).

3. Dependence of the path selection on V_{max}

a. Case with flat bottom

The numerical integration was performed as follows in the FB case. A straight path was spun up from the initial state with V_{max} increased linearly from 0.10 to 0.80 m s^{-1} in 150 days and maintained for 650 days afterward. Starting with this straight path, the dependence of the path selection on V_{max} was investigated with a monotonic change of V_{max} in 30~200 days.

Figure 2 shows the distance of the Kuroshio axis from the southern coast of Japan for various V_{max} in the FB case. It is defined by a maximum distance for a meandering-path (C-type-path) state, or meander amplitude, and by the minimum one along a line **S** off Enshunada (Fig. 1) for a straight-path state. Since the distance exhibits a significant temporal oscillation in some cases, the mean value over an oscillation period is plotted by a solid or open circle with an error bar showing the standard deviation. The dependence of the path selection on V_{max} is basically the same as in the barotropic case (AMA97). That is, three regimes appear according to the magnitude of V_{max}: regime I with a straight path (indicated by ○) at low velocities (V_{max} < 0.60 m s^{-1}), regime II with a meandering path (●) at high velocities (V_{max} > 1.00 m s^{-1}), and regime III with both straight and meandering (or C-type) paths at intermediate velocities (0.60 ≤ V_{max} ≤ 1.00 m s^{-1}). As in the barotropic case, a C-type path (⊙) appears at the lower end of regime III though the range of V_{max} for this path is widened (0.60 ≤ V_{max} ≤ 0.65 m s^{-1}). (The reason will be discussed later.)

Figure 3 shows the distributions of the "pseudo" transport function ψ in each layer for four typical paths. The "pseudo" transport function ψ_i for the ith layer at position P is defined by

$$\int_{P_0}$$

where $\mathbf{u}_i$ is the velocity vector, h_i' the thickness of the layer, $d\mathbf{l}$ a vector line element along the integral path, $\mathbf{k}$ the unit vector directing upward, and P_0 the reference position, which is set at the northeastern corner of the basin. The current in each layer flows approximately along the contour lines of ψ since the interface displacement η does not change so abruptly.

The flow basically concentrates in the upper layer, where the dynamical balance along the current path is the same as in the barotropic case (Akitomo et al. 1991;AMA97).

In the lower layer, the flow is weak except that relatively strong anticyclonic and cyclonic circulations appear off Shikoku and Enshunada, respectively, accompanied with a meandering path (Figs. 3f and 3h). These circulations agree with observations during meandering-path years (Ishii et al. 1983; Sekine et al. 1985).

Despite the above similarities to the barotropic case, the range of regime III shifts to higher velocities by 0.10~0.30 m s^{-1}. According to Akitomo et al. (1991), the upper limit of regime III is determined by the behavior of a small meander formed southeast of Kyushu. A straight path continues to be maintained as long as a small meander stagnates southeast of Kyushu, whereas it changes into a meandering path when a small meander becomes progressive with increasing V_{max}. On the other hand, the lower limit of regime III is controlled by the strength of the vorticity supplied from the southern coast of Japan as well as from the tip of Kyushu. A meandering path can exist when V_{max} is so high that the vorticity supply can be strong enough to maintain it. Otherwise, a meandering path shrinks into a straight path. Thus, to clarify the reason for the range shift of regime III in the two-layer case, we need to examine how stratification affects the behavior of a small meander and intensity of the vorticity supply from the coast.

Figure 4 shows the current axis in a straight-path state when V_{max} = 0.70 m s^{-1} for the two-layer (solid curve) and the barotropic (dashed curve) case (Fig. 4a), and the interface depth along it in the two-layer case (Fig. 4b). As clearly seen from Fig. 4a, a small meander southeast of Kyushu is larger in the two-layer case than in the barotropic case, while the position of the current axis is nearly the same in other regions.

Corresponding to this enlargement of a small meander, the interface depth largely changes around Kyushu. (Its gradual shoaling from upstream to downstream over the whole basin is due to the different depths between the inlet and the outlet.) After deepening toward point **A** (Fig. 4), the interface abruptly shallows by about 5 m toward the western coast of Kyushu (indicated by a large arrow between points **A** and **B**) and again deepens gradually around the enlarged small meander. The shoaling of the interface west of Kyushu is because the main flow directing toward the coast there ascends the slope of the interface.

From the viewpoint of potential vorticity conservation, this abrupt shoaling is expected to produce negative relative vorticity and to increase the radius of curvature of the current path. Quantitatively, shoaling of about 5 m can increase the radius by about 50 km, assuming that other factors are unchanged. The radius southwest of Kyushu, estimated from the 100-km-long segment of the current path centered at point **B**, is about 285 km in the two-layer case while about 225 km in the barotropic case. Since the radius is almost the same in the upstream region between the two cases (around point **A**; ~135 km), the difference at point **B**, ~60 km, can be explained by the shoaling of the interface. Further, the subsequent deepening of the interface around the enlarged small meander (southeast of Kyushu) acts to diminish the radius of curvature. As a result, the current path returns to the same position as in the barotropic case downstream of point **C**. Therefore, the enlarged small meander is stably maintained. This in turn leads to the maintenance of a straight path through the reduction of the vorticity supply from the southern coast of Kyushu. Although such a change of the interface (thermocline) around Kyushu has not so far been reported in the actual sea, it seems to be necessary to investigate the detailed structure of stratification around Kyushu for clarification of its effect on the behavior of a small meander, or the Kuroshio path variation.

In the meandering-path state, the offshore shift of the current axis compared with the barotropic case is also found along the southern coast of Shikoku or Honshu (e.g., Fig. 3b). This reduces the positive vorticity supply from the southern coast of Japan to shift the lower limit of a meandering path to higher V_{max}. Figure 5 shows the corresponding difference of the alongcoast position of the meandering segment between the two-layer and the barotropic case. The range in which the alongcoast position of the meandering segment decreases with V_{max} shifts to higher V_{max} by about 0.15 m s^{-1} in the two-layer case ($V_{max} \leqslant$ 0.90 m s^{-1}: solid circle), compared with the barotropic case ($V_{max} \leqslant$ 0.75 m s^{-1}: solid square). This means that higher V_{max} is needed to maintain a meandering path in the two-layer case.

Another feature found in Fig. 5 is that there appears a meandering path maintained only by the vorticity supply from

the tip of Kyushu in regime III (0.90 $\leqslant V_{max} \leqslant$ 1.00 m s^{-1}); such a meandering path appears only in regime II in the barotropic case. This corresponds to the fact that a small meander stagnating southeast of Kyushu extends the range of regime III up to V_{max} = 1.00 m s^{-1} in the two-layer case, as mentioned above. Thus, the boundary between regimes II and III is determined by the behavior of a small meander, that is, stagnant or progressive, not by the difference in the mechanism maintaining a meandering path.

In conclusion, stratification has the effect of stably maintaining an enlarged small meander southeast of Kyushu through the interface change south of Kyushu. Therefore, a straight path can exist at higher V_{max} compared with the barotropic case. On the other hand, a meandering path needs higher V_{max} for its maintenance since the current path is shifted offshore.

Stratification changes more features of the flow. As mentioned before, a C-type path appears for a finite range of V_{max} at the lower end of regime III. Its amplitude is about 300 km (Fig. 6), which is somewhat larger than that in the barotropic case (Fig. 3 in AMA97). A C-type path is essentially maintained by the geometrical effect of Hachijo Island (AMA97). Stratification enlarges and stabilizes it through shoaling of the interface depth around Hachijo Island, as around Kyushu (indicated by an arrow in the lower panel of Fig. 6). Further, stratification leads to significant temporal variation of the meandering path associated with eddy shedding (see error bars in Fig. 2; e.g., Yoon and Yasuda 1987). The interface deepens around the tip of the meandering segment and positive vorticity is produced through potential vorticity conservation to accelerate the detachment of a cyclonic eddy.

b. Case with bottom topography

Next, we examine the dependence of the path selection on V_{max} in the BT case. The result shown in Fig. 7 is strikingly different from the barotropic case (Akitomo et al. 1991; AMA97) and the FB case (Fig. 2). A straight path (indicated by ○) appears for the whole experimental range of V_{max} and a meandering path (●) only at intermediate V_{max}. As a result, three regimes of the path selection are classified as follows. Regime I with a straight path appears at low velocities (V_{max} < 0.65 m s^{-1}; Fig. 8a), regime II with a straight path (not a meandering path) at high velocities (V_{max} > 1.10 m s^{-1}; Fig. 8b), and regime III with both straight and meandering (C-type) paths at intermediate velocities (0.65 $\leqslant V_{max} \leqslant$ 1.10 m s^{-1}; Figs. 8c and 8d). C-type paths appearing at the lower end of regime III (⊙; 0.65 $\leqslant V_{max} \leqslant$ 0.70 m s^{-1}; not shown) are the same as in the FB case.

The flow concentrates in the upper layer, as in the FB case. The overall flow patterns in the upper and lower layers are similar to those in the FB case for regimes I and III (cf. Figs. 3 and 8). In the lower layer, however, a flow going along the isobath appears and it is concentrated on the slope region south of Japan. Particularly, anticyclonic and cyclonic circulations accompanied with a meandering path are distorted (Fig. 8h). The former is captured by continental slope east of Kyushu and the latter is located in the flat-bottom (4000 m) region offshore.

In regime II, a straight path shows significant temporal changes accompanied with eddy motions in both layers (Figs. 8b and 8f). As a result, the Kuroshio axis south of Japan fluctuates around its mean position by several tens of kilometers (the standard deviation) as shown in Fig. 7. Nevertheless, a straight path in regime II can be considered to be stochastically stable since it is maintained for a long time; for example, more than 3000 days when V_{max} = 1.30 m s^{-1} (Figs. 8b and 8f).

The most noticeable differences of the BT case from the other cases are that a meandering path disappears at high velocities and that a straight path appears for the whole experimental range of V_{max}; in other words, the Kuroshio takes only a straight path at high velocities (regime II). As discussed in the last subsection, the fate of a straight path given an increase in V_{max} is determined by the behavior of the small meander formed southeast of Kyushu. From this point of view, small meanders, which continually appear southeast of Kyushu to progress eastward, do not develop into a meandering path but leave the southern coast of Japan as in the case with V_{max} = 1.30 m s^{-1} (Fig. 9). To examine the reason for this, Fig. 10 shows the distance of the current axis south of Kyushu (the distance from the southern coast of Kyushu along a line **K**; Fig. 9). Comparing with the FB case (not shown), the current axis is located about 5 km onshore in a straight-path state since the continental slope captures the main current. The similar onshore shift is found south of Japan (Shikoku or Honshu). As mentioned before (Fig. 8), the current under the Kuroshio is significantly affected by the bottom topographic features. It flows onshore, concentrated on the continental slope region south of Japan, whereas it shifts offshore and disperses in the FB case (Fig. 3). This, in turn, causes the Kuroshio main current in the upper layer to follow an onshore path along the continental slope through interface change. Thus, the development of a small meander is

prevented, even at higher V_{max} ($V_{max} \geq 1.10$ m s^{-1}). However, it should be noted that the onshore shift of the current path has an opposite effect to develop a small meander through the increased vorticity supply from the coast. This is the reason why a significant temporal change appears, accompanied with repeated eastward progression of small meanders (Figs. 7, 8, and 9).

Next, we turn to the mechanism by which the range of a meandering path is determined. The onshore shift of the current path south of Kyushu (Fig. 9) is also a key factor in controlling the range of the meandering-path state. Figure 11 shows the alongcoast position of the meandering segment against V_{max}. As seen from this figure, the range in which the meandering path is maintained only by vorticity supply from the tip of Kyushu appears when $V_{max} \geq 0.80$ m s^{-1} whereas it did so when $V_{max} \geq 0.90$ m s^{-1} in the FB case (Fig. 5). This means that the onshore path increases the vorticity supply from the south coast of Kyushu in the BT case. Further, when $V_{max} \geq 0.90$ m s^{-1}, the alongcoast position of the meandering segment shifts downstream by about 100 km compared with the FB case. It is this downstream shift that causes the range of a meandering path, or regime III, to be narrower at its upper end since the Izu Ridge is essentially a nodal point restricting the downstream shift of a meander state (White and McCreary 1976).

The difference in the alongcoast position between the BT and FB cases for $V_{max} \geq 0.90$ m s^{-1} seems inconsistent with the theory that predicts that it is proportional to $(V_{max}/\beta)^{1/2}$ for a meandering path maintained as a Rossby lee wave. This is because of the different positions of the current path south of Kyushu between the two cases (Fig. 10). The offshore path south of Kyushu reflects the fact that the current direction turns southward since the current is located at almost the same position off the southwest corner of Kyushu. Figure 12, comparing the two current axes with $V_{max} = 0.90$ m s^{-1}, clearly demonstrates that the difference in the position of current axis, or the flow direction, south of Kyushu affects the behavior downstream, that is, the onshore path south of Kyushu causes an eastward shift of the meandering segment in the BT case.

Further examination of Fig. 7 makes it clear that the value of V_{max} giving the lower end of the range of a meandering path, or regime III, becomes larger by 0.10 m s^{-1}, although the meandering segment is located farther upstream in this case than in the barotropic or FB case at the lower end of regime III (cf. Figs. 5 and 11). This is also due to the influence of the Izu Ridge since the flow ascending the western slope of the ridge cannot remain there stably. Thus, the narrowing of regime III at its lower end is due to a mechanism different from the FB case.

The effects of bottom topography are summarized as follows. Since the continental slope south of Japan acts to capture the Kuroshio, a small meander cannot develop into a large meander despite that the onshore current path induces a significant vorticity supply from the coast. Thus, a straight path becomes possible for the whole experimental range of V_{max}. The Izu Ridge is another important feature in determining the range of regime III, by preventing the Kuroshio current from taking a meandering path hanging over it at both ends of regime III.

4. Path transitions due to monotonic velocity changes

a. Case with flat bottom

Next, we investigate the transition processes between a straight and a meandering path when monotonic changes of V_{max} are imposed in the FB case. These transitions are basically the same as in the barotropic case (Akitomo et al. 1991; AMA97). A straight path changes into a meandering (straight) path when V_{max} increases to regime II. In this transition, a small meander formed southeast of Kyushu progresses eastward along the southern coast of Japan to develop into a large meander off Enshunada in 100~150 days. In the reverse transition, a meandering path changes into a straight path via a C-type path with a decrease in V_{max} from regime II (III) to regime I. It takes about 1000 days when V_{max} decreases from 0.80 to 0.50 m s^{-1} in 30 days; this is not so different from the barotropic case.

Nevertheless, some differences are found in the transition process from a straight to a meandering path. Figure 13 shows the temporal change of ψ in the upper layer when V_{max} increases from 0.70 to 1.10 m s^{-1} in 30 days (from day 5800 to 5830). The small meander formed just after the increase in V_{max} develops southeast of Kyushu (day 5850; Fig. 13b) to progress eastward (day 5890 and 5910; Figs. 13c and 13d) and changes into a large meander off Enshunada (day 5970; Fig. 13e). After that, the meandering path is almost stably maintained (Fig. 13f). The transition takes only 170 days after the start of velocity change. This is a great contrast to the barotropic case in which the same transition takes

more than 600 days after the start of velocity change (AMA97). This difference is because the small meander is enlarged much more by the influence of baroclinicity of the flow as discussed in the last section.

Another difference from the barotropic case is related to the magnitude of velocity change. Figure 14 shows the result with an increase in V_{max} from 1.00 to 1.10 m s^{-1} in 30 days. After the increase in V_{max}, small meanders appear one after another and progress eastward to leave the domain of interest, not to develop into a large meander, till day 4500 (1700 days after the start of velocity change). After that, the small meander formed on day 4690 develops into a C-type path, not a meandering path (not shown). Though this C-type path seems to be an artificial result since it is largely affected by the sidewalls around the outlet of the experimental domain, the two cases obtained here (Figs. 13 and 14) imply that different magnitudes of velocity change may lead to different final states. This is also in contrast to the barotropic case, in which the path transition from a straight to a meandering path occurs whenever V_{max} increases up to regime II (Akitomo et al. 1991).

As discussed before, baroclinicity of the flow causes the offshore shift of the current path. This can lead to two different results since the offshore current path has two effects oppositely operating on the development of small meander: to enlarge a small meander and to reduce the vorticity supply from the coast. With a large velocity change, the quick transition from a straight to a meandering path can occur (Fig. 13) since the effect of an enlarged small meander exceeds the reduction of vorticity supply from the coast. Otherwise, the formation and the eastward progression of a small meander continues and does not lead to the transition to a meandering state (Fig. 14).

b. Case with bottom topography

Since the dependence of the path selection on V_{max} in the BT case is different from those in the barotropic and FB case (Fig. 7), the path transition by a monotonic change of V_{max} is also different. The transition from a straight to a meandering path due to a monotonic velocity change never occurs because of the appearance of a straight path for the whole experimental range of V_{max}. Instead, this transition needs a short-term increase in V_{max}, as discussed in Part II (Masuda and Akitomo 1999). This is not inconsistent with recent observational studies implying that a short-term increase of the current velocity causes the transition from a straight to a meandering path (e.g., Kawabe 1995; Akitomo et al. 1996).

On the other hand, the transition from a meandering to a straight path with a decrease in V_{max} from regime III to I occurs in the same manner as in the barotropic and FB case, including the appearance of a C-type path in the course of this transition. It takes about 1000 days when V_{max} is reduced from 0.80 to 0.55 m s^{-1}. Hence, it is concluded that bottom topography does not affect the reverse transition due to a decrease in V_{max}. With an increase in V_{max} from regime III (1.10 m s^{-1}) to II (1.20 m s^{-1}) in 200 days, the transition to a straight path also occurs. However, it is largely affected by the sidewalls since significant time variations cover the whole basin. An experiment with a larger model basin is needed to examine this transition process in detail.

5. Summary

We have investigated the effects of stratification and bottom topography on the Kuroshio path variation south of Japan, executing numerical experiments with a two-layer inflow–outflow model. In this study (Part I), our attention is focused on the dependence of the path selection on the velocity V_{max} and the path transition by monotonic velocity changes.

In the FB case, the dependence of the path selection on V_{max} is basically the same as in the barotropic case (e.g., AMA97). The Kuroshio takes a straight path at low velocities (V_{max} < 0.60 m s^{-1}), a meandering path at high velocities (V_{max} > 1.00 m s^{-1}), and both straight and meandering (C-type) paths at intermediate velocities (0.60 m s $\leqslant V_{max} \leqslant$ 1.00 m s^{-1}; multiple equilibrium regime). A C-type path appears at the lower end of the multiple equilibrium regime (0.60 $\leqslant V_{max} \leqslant$ 0.65 m s^{-1}). However, the range of the multiple equilibrium regime shifts toward higher velocities by 0.10~0.30 m s^{-1}, compared with the barotropic case. Stratification causes the offshore shift of the current axis especially south of Kyushu through the conservation of potential vorticity in the upper layer. This in turn reduces the vorticity supply from the coast. A stagnating small meander southeast of Kyushu becomes larger and a straight path does not change into a meandering path even for higher V_{max}. On the other hand, the reduction of vorticity supply means that higher V_{max} is needed for the maintenance of a meandering path.

The addition of bottom topography changes the dependence of the path selection on V_{max} drastically. A straight path appears for the whole experimental range of V_{max} while a meandering path appears only at intermediate V_{max} with C-type paths at the lower end of the meandering-path state. Three regimes of the path selection are classified; two straight-path regimes at low velocities ($V_{max} < 0.65$ m s^{-1}) and at high velocities ($V_{max} > 1.10$ m s^{-1}), and the multiple equilibrium regime at intermediate velocities ($0.65 \leqslant V_{max} \leqslant 1.10$ m s^{-1}). The value of V_{max} for the lower end of a meandering path also becomes larger (0.73 m s^{-1}) than that in the barotropic case by 0.20 m s^{-1}. Since the continental slope from Kyushu to Shikoku causes the Kuroshio to flow on the nearshore path, a small meander formed southeast of Kyushu cannot develop adequately into a larger meander at any V_{max} despite the larger vorticity supply from the coast. The Izu Ridge acts to inhibit a meandering path hanging over its western slope. Then, the range of a meandering-path state, or regime III, becomes narrower at its both ends.

The transition processes between a straight and a meandering path due to monotonic changes of V_{max} are basically the same as in the barotropic case. That is, a straight (meandering) path changes into a meandering (straight) path only when a straight (meandering) path cannot exist. However, there are some exceptions. In the FB case, different final states can be realized for different magnitudes of velocity change. This is because the offshore path of the Kuroshio due to baroclinicity has two effects oppositely operating on the path transition, that is, to enlarge a small meander and to reduce the vorticity supply from the coast. Another difference from the barotropic case is that the transition from a straight to a meandering path with monotonic changes of V_{max} never occurs in the BT case because a straight path appears for the whole experimental range of V_{max}. For this transition, a short-term increase in V_{max} is needed (Part II).

The dependence of the path selection on V_{max} in the BT case (Fig. 7) is similar to the result obtained in a barotropic ocean model with the Izu Ridge by Chao (1984). In his experiment, the transition from a straight to a meandering path occurs with a monotonic decrease in volume transport. During the transition, small meanders generated east of Kyushu at a 40-day interval progress eastward one after another and pile up to form a large meander to the west of the Izu Ridge. Hence, to examine the possibility of the similar transition, a decrease in V_{max} from 1.20 to 0.90 m s^{-1} in 30 days was imposed on a straight-path state in regime II (not shown). However, no path transition occurs though a small meander appears southeast of Kyushu to progress eastward several times. This different result from Chao's is because the continental slope along the southern coast of Japan prevents a small meander from developing in the present experiment and because a narrow passage between the southern coast of Japan and the Izu Ridge acts to allow the pileup of small meanders progressing from upstream in Chao's experiment. From the observational point of view, it is emphasized that such a pileup of small meanders due to a decrease in volume transport has not been reported during the transition. Rather, recent studies based on observations suggest that a short-term increase of velocity may cause the path transitions (e.g., Kawabe 1995; Akitomo et al. 1996).

Despite many interesting results about the effects of stratification and bottom topography on the Kuroshio path selection, it should be noted that the model ocean is confined to the south of Japan and the East China Sea, and that stratification and bottom topography is highly simplified. Thus, to reach a decisive conclusion about this problem, further study with a more realistic model ocean is needed. Nevertheless, many similarities to observations, which will be presented in Part II, show that the present results can shed some light on the dynamics of the Kuroshio path variation south of Japan. In Part II, we will investigate the role of a short-term increase of velocity in the Kuroshio path transitions focusing on the behavior of small meander, which is an important factor to control the transitions and discuss the applicability to the actual ocean (Masuda and Akitomo 1999).

Acknowledgments

The numerical calculation was carried out on FACOM M1800 and VP2600 in the Data Processing Center of Kyoto University. A part of this study has been supported by CREST (Core Research for Evolutional Science and Technology) of Japan Science and Technology Corporation (JST).

REFERENCES

Akitomo, K., T. Awaji, and N. Imasato, 1991: Kuroshio path variation south of Japan. Part 1: Barotropic inflow–outflow model. *J. Geophys. Res.*, **96,** 2549–2560..

— , M. Ooi, T. Awaji, and K. Kutsuwada, 1996: Interannual variability of the Kuroshio transport in response to the wind stress field over the North Pacific: Its relation to the path variation south of Japan. *J. Geophys. Res.*, **101,** 14 057–14 071..

— ,S. Masuda, and T. Awaji, 1997: Kuroshio path variation south of Japan: Stability of the paths in a multiple equilibrium regime. *J. Oceanogr.*, **53,** 129–142..

Chao, S.-Y., 1984: Bimodality of the Kuroshio. *J. Phys. Oceanogr.*, **14,** 92–103.. Find this article online

Endoh, M., 1978: Effects of a marine ridge to western boundary current in a three-dimensional source-sink flow model. *J. Oceanogr. Soc. Japan*, **34,** 303–306..

Ishii, H., Y. Sekine, and Y. Toba, 1983: Hydrographic structure of the Kuroshio large meander-cold water mass region down to the deeper layers of the ocean. *J. Oceanogr. Soc. Japan*, **39,** 240–250..

Kawabe, M., 1980: Sea level variations around the Nansei Islands and the large meander in the Kuroshio south of central Japan. *J. Oceanogr. Soc. Japan*, **36,** 227–235..

— ,1985: Sea level variations at the Izu Islands and typical stable path of the Kuroshio. *J. Oceanogr. Soc. Japan*, **41,** 307–326..

— ,1987: Spectral properties of sea level and time scales of Kuroshio path variations. *J. Oceanogr. Soc. Japan*, **43,** 111–123..

— ,1995: Variations of current path, velocity, and volume transport of the Kuroshio in relation with the large meander. *J. Phys. Oceanogr.*, **25,** 3103–3117.. Find this article online

Kutsuwada, K., 1988: Interannual correlation between sea level difference at the south coast of Japan and wind stress over the North Pacific. *J. Oceanogr. Soc. Japan*, **44,** 68–80..

Masuda, A., 1982: An interpretation of the bimodal character of the stable Kuroshio path. *Deep-Sea Res.*, **29,** 471–484..

Masuda, S., and K. Akitomo, 1999: Effects of stratification and bottom topography on the Kuroshio path variation south of Japan. Part II: Path transitions in a multiple equilibrium regime. *J. Phys. Oceanogr.*, in press..

Mizuno, S., K. Kawatate, T. Nagahama, and A. Kaneko, 1990: Time variation of Kuroshio currents in the East China Sea (in Japanese). *Sea Sky*, **66,** 163–180..

Nishida, H., 1982: Description of the Kuroshio meander in 1975–1980—Large meander of the Kuroshio in 1975–1980. *Rep. Hydrogr. Res.*, **17,** 181–207..

Nishizawa, J., E. Kamihira, K. Komura, R. Kumabe, and M. Miyazaki, 1982: Estimation of the Kuroshio mass transport flowing out of the East China Sea to the North Pacific. *La Mer*, **20,** 55–59..

Nitani, H., 1972: Beginning of Kuroshio. *Kuroshio–Its Physical Aspects*, H. Stommel and K. Yoshida, Eds., University of Tokyo Press, 129–163..

— ,1975: Variation of the Kuroshio south of Japan. *J. Oceanogr. Soc. Japan*, **31,** 154–173..

— ,1977: Process of the occurrence, continuation and disappearance of the large meander of the Kuroshio off Enshu-nada (in Japanese). *Mar. Sci. Mon.* (*Kaiyo Kagaku*), **9,** 29–36..

Obata, A., 1993: The relation between Kuroshio transport and path south off Honshu (in Japanese). Kuroshio Exploitation and Utilization Research, Rep., Japan Science and Technology Agency, Tokyo, Japan, 44–55..

Qiu, B., and T. M. Joyce, 1992: Interannual variability in the mid- and low-latitude western North Pacific. *J. Phys. Oceanogr.*, **22,** 1062–1079.. Find this article online

Robinson, A. R., and B. Taft, 1972: A numerical experiment for the path of the Kuroshio. *J. Mar. Res.*, **30,** 65–101..

Saiki, M., 1982: Relation between the geostrophic flux of the Kuroshio in the eastern China Sea and its large-meanders in south of Japan. *Oceanogr. Mag.*, **32,** 11–18..

— ,1985: Transport of the Kuroshio (in Japanese). *Mar. Sci. Mon. (Kaiyo Kagaku)*, **17,** 267–273..

Sekine, Y., 1990: A numerical experiment on the path dynamics of the Kuroshio with reference to the formation of the large meander path south of Japan. *Deep-Sea Res.*, **37,** 359–380..

— ,and Y. Toba, 1981: Velocity variation of the Kuroshio during the small meander formation south of Kyushu. *J. Oceanogr. Soc. Japan*, **37,** 87–93..

— ,H. Ishii, and Y. Toba, 1985: Spin-up and spin-down processes of the large cold water mass of the Kuroshio south of Japan. *J.*

Oceanogr. Soc. Japan, **41,** 207–212..

Shoji, D., 1964: A note on the abnormalous cold water regions along the Japanese coasts and their relation to the fluctuations in the current speeds of the Kuroshio (in Japanese). *Bull. Japan Soc. Fish. Oceanogr.*, **4,** 31–40..

— ,~~1~~1972: Time variation of the Kuroshio south of Japan. *Kuroshio—Its Physical Aspects*, H. Stommel and K. Yoshida, Eds., University of Tokyo Press, 217–234..

White, W. B., and J. P. McCreary, 1976: On the formation of the Kuroshio meander and its relationship to the large-scale ocean circulation. *Deep-Sea Res.*, **23,** 33–47..

Yasuda, I., J.-H. Yoon, and N. Suginohara, 1985: Dynamics of the Kuroshio large meander—Barotropic model. *J. Oceanogr. Soc. Japan*, **41,** 259–273..

Yoon, J.-H., and I. Yasuda, 1987: Dynamics of the Kuroshio large meander: Two-layer model. *J. Phys. Oceanogr.*, **17,** 66–81.. Find this article online

---

Tables

Table 1. Physical parameters used in the present experiment.

Parameter	Symbol	Value
Coriolis parameter, s^{-1}	f_0	6.15×10^{-5}
Beta parameter, $s^{-1}\ m^{-1}$	β	1.95×10^{-11}
Acceleration due to gravity, $m\ s^{-2}$	g	9.8
Horizontal viscosity, $m^2\ s^{-1}$	ν_H	5.0×10^2
Inclination angle of the south coast of Japan, deg	θ	20
Grid size, m	$\Delta x, \Delta y$	1.0×10^4
Density difference, $kg\ m^{-3}$	$\Delta\rho$	3.0
Upper-layer thickness at rest, m	h_1	800
Maximum total depth, m	D_0	4000
Time increment, s	Δt	720 ~ 960

Click on thumbnail for full-sized image.

Figures

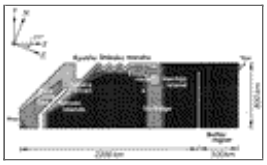

Click on thumbnail for full-sized image.

Fig. 1. Model basin used in the present experiment. Shaded regions show water depths of 1300, 2000, 3000, 4000 m from lighter to darker. Horizontal geometry is the same as in AMA97 except that the buffer region is added to the downstream side. Line **S** off Enshunada is indicated by the white dashed line, on which the distance of the Kuroshio axis from the southern coast of Japan for straight path is examined in Fig. 2.

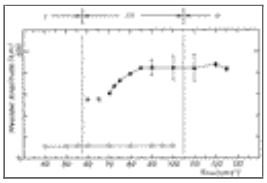

Click on thumbnail for full-sized image.

Fig. 2. Distance of the Kuroshio axis from the southern coast of Japan against V_{max} in the FB case. Symbols (○), (●), and (⊙) indicate a straight, a meandering, and a C-type path, respectively. Error bars show a standard deviation of the temporal oscillation.

Click on thumbnail for full-sized image.

Fig. 3. “Pseudo” transport function ψ (see text for its definition) for typical paths in each regime in the FB case. (a) and (e) Straight path in regime I (V_{max} = 0.40 m s^{-1}), (b) and (f) meandering path in regime II (1.10 m s^{-1}), (c) and (g) straight path in regime III (0.80 m s^{-1}), and (d) and (h) meandering path in regime III (0.80 m s^{-1}). Left-hand panels are for the upper layer, and those on the right for the lower layer. Contour interval is 4 × 10^{6} m^{3} s^{-1}. Shaded region indicates negative value.

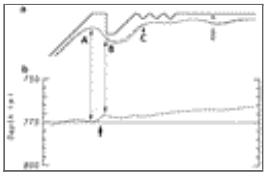

Click on thumbnail for full-sized image.

Fig. 4. (a) The Kuroshio axes in a straight-path state at V_{max} = 0.70 m s^{-1} for the FB case (solid curve) and the barotropic case (dashed curve). (b) Interface depth along the current axis in the FB case. Large arrow indicates the abrupt shoaling of interface depth southwest of Kyushu. Point **A** (**B**) is the upstream (downstream) end of the abrupt shoaling, point **C** the position downstream of which the current path is almost the same as in the barotropic case.

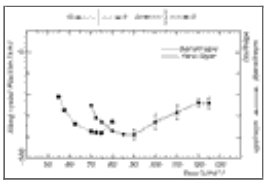

Click on thumbnail for full-sized image.

Fig. 5. Alongcoast position of a large meander against V_{max} in the FB case compared with the result of the barotropic case (AMA97). Symbols and error bars are the same as in Fig. 2.

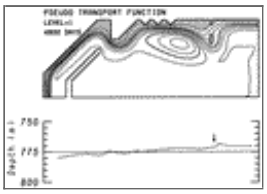

Click on thumbnail for full-sized image.

Fig. 6. Pseudo transport function ψ in the upper layer and interface depth along the current axis for a C-type path with V_{max} = 0.60 m s^{-1} in the FB case. Contour interval as in Fig. 3.

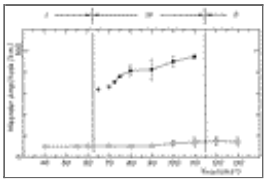

Click on thumbnail for full-sized image.

Fig. 7. As in Fig. 2 but for the BT case.

Click on thumbnail for full-sized image.

Fig. 8. As in Fig. 3 but for the BT case. (a) and (e) Straight path in regime I (V_{max} = 0.40 m s^{-1}), (b) and (f) straight path in regime II (1.30 m s^{-1}), (c) and (g) straight path in regime III (0.80 m s^{-1}), and (d) and (h) meandering path in regime III (0.80 m s^{-1}).

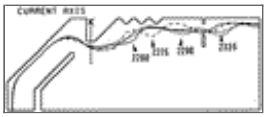

Click on thumbnail for full-sized image.

Fig. 9. Temporal change of the Kuroshio axis with V_{max} = 1.30 m s^{-1} in the BT case. Solid, dashed, dotted, and dash–dotted lines indicate the axes on day 2260, 2275, 2290, and 2335, respectively. Line **K** is indicated by the thick dashed line, on which the distance of the Kuroshio axis from the southern coast of Kyushu is examined in Fig. 10.

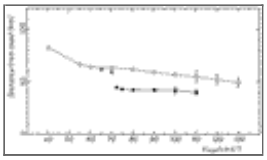

Click on thumbnail for full-sized image.

Fig. 10. Distance of the Kuroshio axis from the southern coast of Kyushu on a line K (Fig. 9) against V_{max} in the BT case. Open circle (○) is for straight paths, solid circle (●) for meandering paths, and (⊙) for C-type paths, respectively. Error bars as in Fig. 2.

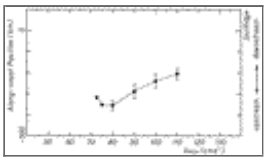

Click on thumbnail for full-sized image.

Fig. 11. As in Fig. 5 but for the BT case.

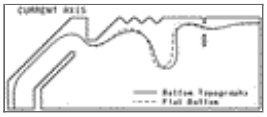

Click on thumbnail for full-sized image.

Fig. 12. The Kuroshio axes in a meandering-path state at V_{max} = 0.90 m s^{-1} in the BT case (solid curve) and the FB case (dashed curve).

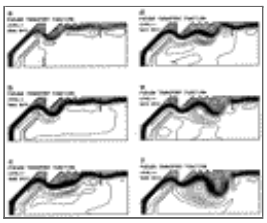

Click on thumbnail for full-sized image.

Fig. 13. Time evolution of pseudo transport function ψ in the upper layer in the FB case when V_{max} increases from 0.70 to 1.10 m s^{-1} in 30 days. (a) Day 5800 (initial), (b) 5850, (c) 5890, (d) 5910, (e) 5970, and (f) 6500. Contour interval is same as in Fig. 3.

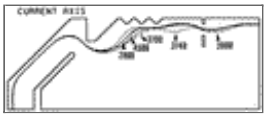

Click on thumbnail for full-sized image.

Fig. 14. Temporal change of the Kuroshio axis in the FB case when V_{max} increases from 1.00 m s^{-1} to 1.10 m s^{-1} in 30 days. Solid, dashed, dotted, dash–dotted, and dash–two-dotted lines indicate the axes on day 2800 (initial), 3700, 3740, 3900, and 4500, respectively.

Corresponding author address: Dr. Shuhei Masuda, Department of Geophysics, Graduate School of Science, Kyoto University, 606-8502 Kyoto, Japan.

E-mail: masuda@kugi.kyoto-u.ac.jp

top